

Electron energy down-conversion in thin superconducting films

A. G. Kozorezov and J. K. Wigmore

Department of Physics, Lancaster University, Lancaster, LA1 4YB, England, United Kingdom

D. Martin, P. Verhoeve, and A. Peacock

Science Payload and Advanced Concepts Office, SCI-A, European Space Agency, ESTEC, Noordwijk, The Netherlands

(Received 18 October 2006; published 29 March 2007)

We have developed a theory of photoelectron energy down-conversion in superconductors in the vicinity of interfaces. Significant differences from the situation in bulk materials arise when the process takes place closer to an interface than the mean free path of pair-breaking phonons. Then some of the energetic phonons generated in the down-conversion cascade can escape from the superconducting film, giving rise to a decrease in the mean number of quasiparticles generated and to statistical fluctuations in that quantity. An additional source of variability is the spatial distribution of the initial photoabsorption sites, giving rise to vertical inhomogeneity. Both effects can be observed in photoabsorption experiments on thin film superconducting tunnel junctions, the former at optical energies and the latter primarily with x rays.

DOI: [10.1103/PhysRevB.75.094513](https://doi.org/10.1103/PhysRevB.75.094513)

PACS number(s): 74.25.Fy, 74.40.+k, 74.50.+r, 85.25.Oj

I. INTRODUCTION

Direct absorption in the electrodes of a superconducting tunnel junction (STJ) is widely used as a mechanism for photon detection because of the high responsivity (charge output per unit energy input) and the simplicity of operation. The basic principle of such a detector is that the energy of the photon absorbed in the superconductor is converted into mobile quasiparticles (QPs), which undergo tunneling to yield a charge output that is directly proportional to the energy of the initial photon. Ideally, the only loss in the system is through the eventual creation of nonproductive phonons having energies below 2Δ , the energy gap of the superconductor, which are unable to break further Cooper pairs. A detailed modeling of the complete energy down-conversion process occurring in an infinite crystal has shown that the fractional loss due to this process is independent of photon energy, amounting to approximately 40% of that quantity. The statistical fluctuations in energy partition between the QPs and subgap phonons also result in uncertainty in the number of generated QPs, or Fano noise. However, such a model is not appropriate for real STJs in which the electrodes are only a few tens of nanometers thick, or in bulk materials when absorption takes place close to an interface. In this situation an additional channel of energy loss is possible via transmission of energetic phonons across the interface with the substrate, before they have been able to generate further QPs. The consequences of this scenario have never previously been considered to our knowledge. In the present paper we describe the analytic modeling of the energy down-conversion process following photon absorption close to an interface, and show that the consequences are reduced charge output and resolution. A preliminary account of the work was published earlier,¹ showing that the signal characteristics of a STJ detector could be significantly degraded under these circumstances. In the present paper we extend the theoretical analysis to more general situations and obtain results which suggest that this mechanism may provide a major contribution toward the unexplained excess noise and spectral broadening observed widely in STJs. In

order to set the context in which the effect of interfaces can be understood, a brief summary of the energy down-conversion process in an infinite crystal will first be given.²⁻⁴

At all but the highest photon energies the total photon energy is transferred to a single photoelectron. On the scale of tens of femtoseconds the photoelectron rapidly shares its excess energy with other electrons via secondary ionization, and plasmon creation and subsequent decay. As a result, after a fraction of a picosecond, the energy of the initial photon has been dispersed into a cloud of mediating electrons each of characteristic energy E_1 . At this energy, typically 1 eV, the electron-phonon interaction begins to dominate over the electron-electron interactions, resulting in almost total conversion of the initial photon energy into a population of phonons with energies of the order of the Debye energy Ω_D , and contained within a well-defined region, known as the phonon bubble. The size of the bubble, typically 10 nm, is determined by the diffusive motion of the intermediate electrons due to emission of successive phonons. The time scale of the $E_1 \rightarrow \Omega_D$ down-conversion stage, t_{dc} , is a key parameter in modeling the effect of down-conversion near surfaces, since it defines the range from which the energetic phonons may reach the interface. The modified down-conversion process that ensues in this region will be described in Sec. II, leading to the phonon density profile in the bubble. The final stage of down-conversion is the excitation of free QPs by absorption of the phonons, initially of energy Ω_D , in the superconducting condensate. However, Ω_D is typically much larger than 2Δ so that the absorption of a high-energy phonon to break a Cooper pair is rapidly followed by the emission of another phonon of lower energy. The process is repeated many times until the energy of the last phonon emitted is too low to excite further QPs. Initially the rate at which this stage proceeds is determined by the phonon pair-breaking rate. However, below a further characteristic energy Ω_1 , the speed of the whole process becomes limited by the rate of emission by the QPs of relaxation phonons which still possess pair-breaking capability. In this stage the pair-breaking mean free path of productive phonons increases with decreasing energy from a few to hundreds of nanom-

eters. Thus the analysis of this complex situation requires a simultaneous modeling of the phonon and electron systems. This will be described in Sec. III, as a result of which the distribution of phonons escaping across the interface will be derived, and hence the energy loss via phonons. The magnitude of the fluctuations in this quantity relates directly to the main observables, phonon noise and vertical inhomogeneity. The existence of a critical cone for phonon transmission across the interface between the relatively soft metal of the electrode and the substrate or barrier, which has much higher acoustic impedance, is of primary importance. Only productive phonons incident on the barrier at angles of incidence less than the critical value are transmitted. Angular fluctuations in the distribution of emitted phonons close to the limiting incident angle of the cone give rise to variations in the number of phonons lost from the STJ. In addition, the number of phonons reaching the interface at angles of incidence within the critical cone depends on the probability of traveling from the point of origin to the escape interface without interacting with the condensate. Because of the spatial distribution of photon absorption sites this gives rise to vertical inhomogeneity of the response. In addition, because of the randomness of interaction with the condensate, this quantity is also subject to statistical fluctuations. Finally, the transmission process itself is probabilistic, providing a further source of statistical fluctuations in the number of transmitted phonons and hence in the measured photon energy.

Both phonon noise and vertical inhomogeneity can be described in terms of contributions to the broadening of a detector response. In Sec. IV predictions of the model are described as a function of incident photon energy for a typical STJ interface, Ta/Al₂O₃, and in Sec. V compared with experimental results at optical and x-ray energies. In addition, some conclusions are drawn regarding the optimization of STJ detectors to obtain maximum resolving power. Although the paper is focused primarily on the effects observed experimentally in STJs, the principles apply equally to any absorption event in a superconductor taking place close to an interface. The application of these principles to transition edge sensor microcalorimeters, in which the superconducting film is both absorber and sensor, is described in Ref. 5.

II. ELECTRON-PHONON DOWN-CONVERSION STAGE $E_1 \rightarrow \Omega_D$: FORMATION OF THE PHONON BUBBLE

Our objective in this section is to obtain expressions for the electron and phonon distribution functions at the end of the $E_1 \rightarrow \Omega_D$ down-conversion stage, together with an estimate of the duration of this stage, t_{dc} . The nonequilibrium state of interacting QPs and phonons is described by the coupled kinetic equations⁶⁻⁹

$$\begin{aligned} \frac{\partial n}{\partial t} - D\Delta n &= I_{ep}\{n, N\} + I_{ee}\{n\} + Q(\epsilon, \mathbf{x}, \mathbf{x}_0, t), \\ \frac{\partial N}{\partial t} &= I_d\{N\} + I_{pe}\{N, n\}. \end{aligned} \quad (1)$$

Here $n=n(\epsilon, \mathbf{x}, t)$ and $N=N(\Omega, \mathbf{x}, t)$ are distribution functions for QPs and phonons, respectively, depending on QP energy

ϵ , phonon energy Ω , position \mathbf{x} , and time t . D is the QP diffusion coefficient, and $I_{ee}\{n\}$, $I_{ep}\{n, N\}$, $I_d\{N\}$, and $I_{pe}\{N, n\}$ are the collision integrals describing, respectively, electron-electron collisions, collisions between QPs and phonons, phonon loss into the substrate, and collisions between phonons and QPs. $Q(\epsilon, \mathbf{x}, \mathbf{x}_0, t)$ is the source term, which depends also on the position of the absorption site \mathbf{x}_0 .

The first-order linear differential equation for the phonon distribution function in (1) can be solved to give $N(\Omega, \mathbf{x}, t)$ in terms of a given QP distribution function. It is straightforward to find the solution for the $E_1 \rightarrow \Omega_D$ stage. As we shall see below, this stage takes place so rapidly² that emitted phonons do not escape from the sample ($I_d\{N\}=0$) or decay, thus forming a phonon cloud with accumulated energy equal to that of the incoming photon. Under these conditions we obtain

$$\begin{aligned} \frac{\partial N(\epsilon, \mathbf{x}, t)}{\partial t} &= \frac{2}{\pi\tau_{ph}} \int_{\Delta}^{\infty} \frac{d\epsilon'}{\Delta} \rho(\epsilon') \rho(\epsilon + \epsilon') \left(1 - \frac{\Delta^2}{\epsilon'(\epsilon + \epsilon')} \right) \\ &\quad \times n(\epsilon + \epsilon', \mathbf{x}, \mathbf{x}_0, t) \\ &\approx \frac{2}{\pi\tau_{ph}} \int_{\Delta}^{\infty} \frac{d\epsilon'}{\Delta} \rho(\epsilon') n(\epsilon', \mathbf{x}, \mathbf{x}_0, t) \\ &= \alpha n(\mathbf{x}, \mathbf{x}_0, t). \end{aligned} \quad (2)$$

Here τ_{ph} is the phonon pair-breaking time, a characteristic parameter of the superconductor, ρ is a dimensionless superconductor density of states, and $n(\mathbf{x}, t) = 2N_0 \int_{\Delta}^{\infty} d\epsilon \rho(\epsilon) n(\epsilon, \mathbf{x}, t)$ is the QP density. N_0 is the density of states in the normal state per spin at the Fermi level, and we have introduced the constant α , which we will define later. Then we have

$$N(\Omega, \mathbf{x}, \mathbf{x}_0, t_{dc}) = \alpha \int_0^{t_{dc}} dt' n(\mathbf{x}, \mathbf{x}_0, t') \quad (3)$$

containing explicitly the dependence on the absorption site position. We must now solve the kinetic equation (1) describing energy loss from E_1 to Ω_D . We choose the source term in the form $Q(\epsilon, \mathbf{x}, \mathbf{x}_0, t) = 1/(2N_0) \delta(t) \delta(\mathbf{x} - \mathbf{x}_0) \delta(\epsilon - E_1)$. Since the rate of down-conversion decreases with decreasing energy the duration of the $E_1 \rightarrow \Omega_D$ stage is mainly determined by evolution in the spectral region close to Ω_D , accompanied by a major expansion of the excited volume. We may start from a lower energy E'_1 , neglecting the slight expansion which occurs during the $E_1 \rightarrow E'_1$ stage, where E'_1 is defined to be the threshold below which the electron-phonon interaction controls both electron energy and momentum relaxation. Then $I_{ee}\{n\}$ in (1) can be neglected. In the term $I_{ep}\{n, N\}$ we eliminate the phonon distribution function using (3). Keeping only the terms describing spontaneous emission of phonons and neglecting all coherence terms in the electron-phonon scattering cross section for the spectral range $\epsilon \geq \Omega_D \gg \Delta$, we obtain

$$\frac{\partial n}{\partial t} - D\Delta n - \frac{\lambda\Omega_D}{4} \hbar \Omega_D \frac{\partial n}{\partial \epsilon} = Q \quad (4)$$

where λ is a dimensionless electron-phonon coupling constant of order unity. Equation (4) describes the spatial diffusion of the electron cloud and the simultaneous spectral transformation. However, to find the phonon distribution function in (2) we need to know only the electron density. Thus, integrating (4) over all electron energies and assuming the diffusion coefficient to be independent of electron energy, we arrive at the diffusion equation describing the density of the electron cloud during the $E'_1 \rightarrow \Omega_D$ stage of the down-conversion cascade. The normalized electron density (in units of $2N_0\Delta$) for electrons diffusing within a layer of thickness d with normal along the z axis ($-d/2 < z < d/2$) is given by

$$n(\mathbf{x}, t) = \frac{1}{2d\pi Dt} \sum_{m=0}^{\infty} \frac{1}{1 + \delta_{m,0}} \cos\left[m\pi\left(\frac{1}{2} + \frac{z}{d}\right)\right] \times \cos\left[m\pi\left(\frac{1}{2} + \frac{z_0}{d}\right)\right] \exp\left(-\frac{m^2\pi^2 Dt}{d^2} - \frac{(\mathbf{r} - \mathbf{r}_0)^2}{4Dt}\right). \quad (5)$$

Here $\delta_{m,m'}$ is the Kronecker symbol, $\mathbf{x}=(z, \mathbf{r})$, and $\mathbf{r}=(x, y)$ is the two-dimensional (2D) vector defining the coordinates in the xy plane, with diffusion starting from \mathbf{x}_0 . Since we are not interested in the distribution of phonons parallel to the xy plane we may integrate $n(\mathbf{x}, t)$ over x and y to obtain an averaged phonon distribution $\tilde{N}=(1/A) \int d\mathbf{r} N(\Omega, \mathbf{x}, \mathbf{x}_0, t_{dc})$, where A is the area of the interface. As a result we obtain

$$\tilde{N}(\Omega, z, z_0, t_{dc}) = \frac{1}{A} \frac{E}{\Omega_D} \frac{8}{\beta\Omega_D^3 d} \sum_{m=0}^{\infty} \frac{\kappa(m^2 \xi^2)}{1 + \delta_{m,0}} \times \cos\left[m\pi\left(\frac{1}{2} + \frac{z}{d}\right)\right] \cos\left[m\pi\left(\frac{1}{2} + \frac{z_0}{d}\right)\right] \quad (6)$$

where we denote $\kappa(x)=\exp(-x)\sinh(x)/x$, and define $\xi^2 = \pi^2 D t_{dc} / 2d^2$, where E is the photon energy, $\beta=3/2\pi^2 \hbar^3 c_s^3$, and c_s is the mean sound velocity in the superconductor. This substitution ensures that the energy at the end of the $E_1 \rightarrow \Omega_D$ stage remains equal to E , defining α from (3). Note that the phonon density profile at t_{dc} is sharper than that of the electrons, since it is the time convolution of the electron density.

To evaluate t_{dc} we will consider further details of the $E_1 \rightarrow E'_1 \rightarrow \Omega_D$ stage. Below E_1 by definition $\tau_{ee} > \tau_s$, where τ_{ee} and τ_s are the electron-electron ($e-e$) and electron-phonon ($e-ph$) scattering times, respectively. Nevertheless close to E_1 each $e-e$ event results in a drop in electron energy by approximately a factor 2, while in the energy range $[E_1, E'_1]$ phonon emission results in a much smaller loss of energy because $\Omega_D \ll E'_1$. Therefore in the spectral interval $[E_1, E'_1]$ energy relaxation is controlled by the slower $e-e$ interactions, while the faster $e-ph$ collisions control momentum relaxation and hence electron diffusion. At energies lower than E'_1 with further decrease of the $e-e$ interaction strength, $e-ph$ interactions finally become dominant for both energy and momen-

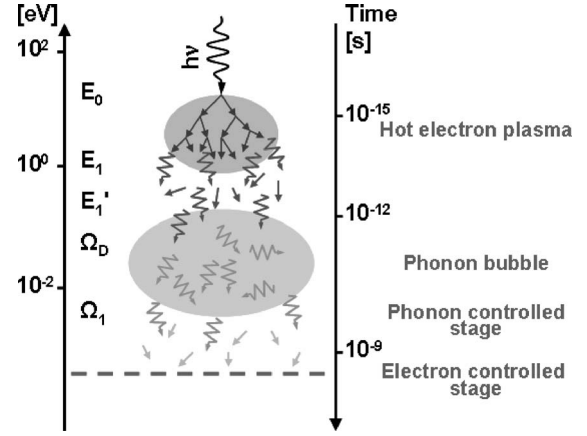


FIG. 1. Schematic picture of photoelectron energy down-conversion in a superconductor.

tum relaxation. During the whole duration of the $E_1 \rightarrow \Omega_D$ stage phonons are emitted across the entire spectrum, and hence the phonon emission time, which determines momentum relaxation, does not depend on the electron energy since $\epsilon > \Omega_D$. In addition the electron group velocity is essentially constant within this energy range above the Fermi level. Thus the electron diffusion coefficient D remains constant and independent of energy, thus justifying the assumptions made above.

The energy E'_1 can be evaluated from the condition

$$\tau_{ee}(E'_1) = \frac{E'_1}{2\Omega_D} \tau_s. \quad (7)$$

Since an electron with energy E'_1 takes on average the same time to lose half its initial energy whether in a single $e-e$ process, or by emitting several $E'_1/2\Omega_D$ phonons (with the emission of each of those phonons taking time τ_s), we obtain from (7)

$$E'_1 = 2^{1/3} E_1^{2/3} \Omega_D^{1/3} \approx \Omega_D \left(\frac{E_1}{\Omega_D}\right)^{2/3} \gg \Omega_D. \quad (8)$$

In arriving at this result we assume that for $\epsilon > \Omega_D$ $e-e$ scattering is not affected by disorder and scales as $\tau_{ee}^{-1} \sim \epsilon^2$. To summarize, a phonon bubble is generated during the $E_1 \rightarrow \Omega_D$ stage. The first substage $E_1 \rightarrow E'_1$ is the faster with an estimated duration of $\tau_{ee}(E'_1)(1/4 + 1/16 + \dots) = \tau_{ee}(E'_1)/3$. The second substage $E'_1 \rightarrow \Omega_D$ takes time $\tau_{ee}(E'_1)/2$ from E'_1 to $E'_1/2$ because there are two equally contributing channels each with the rate $\tau_{ee}(E'_1)^{-1}$, and a further $\tau_{ee}(E'_1)/2$ for phonon emission to relax the electron energy from $E'_1/2$ to Ω_D . Thus our result for the duration of the $E_1 \rightarrow \Omega_D$ stage is

$$t_{dc} = \frac{4}{3} \tau_s \left(\frac{E_1}{E'_1}\right)^2 = \frac{1}{3} \left(\frac{4E_1}{\Omega_D}\right)^{2/3} \tau_s. \quad (9)$$

This parameter is important in determining the distance from an interface over which phonon loss can occur, as discussed in Sec. III. The whole down-conversion process is summarized in Fig. 1.

III. PHONON LOSS THROUGH INTERFACES: PHONON NOISE AND VERTICAL INHOMOGENEITY

Having obtained the spatial profile of the phonon distribution function in (6) we are now in a position to calculate phonon losses through the escape interfaces. The difference between down-conversion in bulk superconductor and that in the vicinity of an interface lies in the fact that some productive phonons are lost through the interface. As a result the eventual number of QPs counted is reduced and also, more significantly, there is an increase in statistical fluctuations about the mean, giving rise to phonon noise. A related effect is the dependence of energy loss on the distance between the absorption site and the escape interface, which causes inhomogeneous broadening, or vertical inhomogeneity. We shall assume that phonons incident on the escape interface are reflected and transmitted with probabilities according to acoustic mismatch laws, but more complicated models of high-frequency phonon transfer across the interfaces, for example, scattering-assisted transmission,¹⁰⁻¹³ can also be easily incorporated. Since the superconductors are invariably softer than the substrates on which the films are grown, or than insulating capping layers, there exists a critical angle for total internal reflection. Only phonons that are incident within the critical cone with angle of incidence not exceeding $\vartheta_c = \arcsin(c_s/c)$ can be transmitted across the interface, where c_s and c are the mean sound velocities in the superconductor and neighboring layer, respectively. Another consequence of the difference in acoustic properties is that the maximum frequency in the phonon spectrum of a superconductor is lower than that of a neighboring layer. Hence all down-conversion phonons incident within the critical cone can leave the superconducting film. The phonon distribution for phonons moving to an interface within the critical angle can be found as a solution of the kinetic equation

$$\frac{\partial \tilde{N}}{\partial t} + c_s \xi \frac{\partial \tilde{N}}{\partial z} + \frac{\tilde{N}}{\tau_{pb}} = \delta(t) \tilde{N}(\Omega, z, z_0, t_{dc}) \quad (10)$$

where ξ is the cosine of the angle between the phonon propagation direction and the z axis, and $\tau_{pb}(\Omega)$ is the phonon lifetime with respect to pair breaking. We will take

$$\tilde{N}(\Omega, \xi, z, z_0, t) = \Theta(t) \tilde{N}(\Omega, z - c_s \xi t, z_0, t_{dc}) \exp[-t/\tau_{pb}(\Omega)] \quad (11)$$

where $\Theta(t)$ is the Heaviside function. Integrating the phonon flux crossing the escape interfaces over the total time taken by all phonons initially generated to reach the escape interfaces, we obtain

$$E_{loss}^{\pm}(z_0) = A \int_0^{\infty} dt \mathbf{q}\left(\pm \frac{d}{2}, t\right) \cdot \mathbf{n}\left(\pm \frac{d}{2}\right) \quad (12)$$

where $\mathbf{q}(z, t)$ and \mathbf{n} are the phonon flux density and outward normal at the escape interfaces, respectively. Substituting (6) for the phonon distribution function we obtain for the total energy lost following the absorption at z_0

$$\begin{aligned} E_{loss}(z_0) &= E_{loss}^+(z_0) + E_{loss}^-(z_0) \\ &= 4E \sum_{m=0}^{\infty} \frac{\kappa(m^2 \xi^2) \cos m\pi(1/2 + z_0/d)}{1 + \delta_{m,0}} \\ &\quad \times \int_0^1 d\xi \xi \eta(m, \xi) \int_0^{\Omega_D} \frac{d\epsilon}{\Omega_D} \left(\frac{\epsilon}{\Omega_D}\right)^3 \frac{l_{pb}(\epsilon)}{d} \\ &\quad \times \frac{\{1 - \exp[im\pi - d/l_{pb}(\epsilon)\xi]\}}{1 + m^2 \pi^2 l_{pb}^2(\epsilon) \xi^2 / d^2} \end{aligned} \quad (13)$$

where $l_{pb}(\epsilon)$ is the phonon mean free path with respect to pair breaks, and the effective transmission coefficient across the two escape interfaces is

$$\eta(m, \xi) = (-1)^m \eta_+(\xi) \Theta(\xi - \xi_c^+) + \eta_-(\xi) \Theta(\xi - \xi_c^-). \quad (14)$$

Here $\xi_c^{\pm} = \cos \vartheta_c^{\pm}$, where ϑ_c^{\pm} are the critical angles and η_{\pm} the transmission coefficients for phonons that are incident on escape interfaces at $z = \pm d/2$, respectively.

To determine the total loss we average over the distribution of photon absorption sites, which depends on the direction of photon incidence. To distinguish between the two incidence geometries we introduce the subscript s , where $s=1$ for incidence across the $z = +d/2$ interface and $s=2$ for incidence across the $z = -d/2$ interface. Then $P_s(z_0, E)$, the normalized probability density for absorption in the film, is

$$P_s(z_0, E) = \frac{\exp\{-[(-1)^s z_0 + d/2]/L(E)\}}{L(E)\{1 - \exp[-d/L(E)]\}} \quad (15)$$

where $L(E)$ is the $1/e$ photon absorption depth. Defining the total energy loss for a particular geometry as $E_{loss}^s = \int_{-d/2}^{d/2} dz_0 P_s(z_0, E) E_{loss}(z_0)$ and calculating the integrals we obtain

$$\begin{aligned} E_{loss}^s &= 4E \sum_{m=0}^{\infty} \frac{\kappa(m^2 \xi^2)}{1 + \delta_{m,0}} \\ &\quad \times \frac{(-1)^{ms} \{1 - \exp[im\pi - d/L(E)]\}}{\{1 - \exp[-d/L(E)]\} [1 + m^2 \pi^2 L^2(E)/d^2]}, \\ &\quad \times \int_0^1 d\xi \xi \eta(m, \xi) \int_0^{\Omega_D} \frac{d\epsilon}{\Omega_D} \left(\frac{\epsilon}{\Omega_D}\right)^3 \\ &\quad \times \frac{l_{pb}(\epsilon)}{d} \frac{1 - \exp[im\pi - d/l_{pb}(\epsilon)\xi]}{1 + m^2 \pi^2 l_{pb}^2(\epsilon) \xi^2 / d^2}. \end{aligned} \quad (16)$$

Fluctuation of E_{loss}^s about its mean arises because of several random processes. First, the number of phonons emitted into the critical cone is subjected to statistical fluctuations. Second, the phonons on their way to the interface interact randomly with the condensate, so that the number reaching the interface also fluctuates. Finally, the transmission of phonons across the interface is a probabilistic process also subjected to fluctuations. The processes described above are independent. Moreover, phonon emission, propagation, and transmission for different frequencies are uncorrelated. This allows us to study the fluctuations by concentrating on the group of phonons from the spectral interval $[\epsilon, \epsilon + d\epsilon]$ propagating inside the critical cone towards an interface. Designat-

ing by dM^\pm the number of phonons in this group and by dM_ϵ^\pm their energy at the initial location z , we write $dM^\pm = \beta \epsilon^2 \tilde{N}(\epsilon, \xi, z, z_0, t_{dc}) d\epsilon$ and $dM_\epsilon^\pm = \beta \epsilon^3 \tilde{N}(\epsilon, \xi, z, z_0, t_{dc}) d\epsilon$. The mean energy that is lost from this group is therefore

$$dM_\epsilon^\pm = \frac{1}{2} \beta \epsilon^3 d\epsilon \int_{\xi_c^\pm}^1 d\xi \eta_\pm(\xi) \exp\left(-\frac{d/2 \mp z}{l_{pb}(\epsilon)\xi}\right) \tilde{N}(\epsilon, \xi, z, z_0, t_{dc}). \quad (17)$$

The factor 1/2 in this expression arises because of the definition of β as an angular averaged quantity, and the exponential factor in the integrand reflects the probability of a phonon reaching the corresponding interface without being absorbed by the condensate.

To calculate the variance of dM_ϵ^\pm we sum up variances due to the independent fluctuation sources and obtain

$$\overline{(\delta dM_\epsilon^\pm)^2} = \overline{(\delta dM_\epsilon^\pm)^2}|_e + \overline{(\delta dM_\epsilon^\pm)^2}|_i + \overline{(\delta dM_\epsilon^\pm)^2}|_t. \quad (18)$$

Here the subscripts e , i , and t are for variances describing phonon emission (into the critical cone), interaction, and transmission fluctuations, respectively. The individual variances may be evaluated as follows. We introduce the energy loss density $e_{loss}^\pm(\epsilon, \xi)$ originating from phonons in the phonon bubble initially at a location z . The expression for this quantity is obtained by integrating the energy flux, obtained from (11) through the (\pm) escape interfaces over time. This gives $e_{loss}^\pm(\epsilon, \xi) = \eta_\pm(\xi) p_\pm'(z, \xi) \beta \epsilon^3 \tilde{N}(\epsilon, \xi, z, z_0, t_{dc})$ where $p_\pm'(z, \xi) = \exp[-(d/2 \mp z)/l_{pb}(\epsilon)\xi]$ is the probability of reaching an interface from point z without interacting with the condensate. The variance for the number of phonons within the energy interval from ϵ to $\epsilon + d\epsilon$ emitted into the critical cone follows a binomial distribution; hence we can write $\overline{(\delta dM)^2} = p_\pm(1-p_\pm)dM$, where we have introduced the probability of emitting a single phonon into the critical cone $p_\pm = 1/2 \int_{\xi_c^\pm}^1 d\xi = \sin^2(\vartheta_c^\pm/2)$. Thus

$$\overline{(\delta dM_\epsilon^\pm)^2}|_e = \frac{1}{2} (1-p_\pm) \beta \epsilon^4 d\epsilon \times \int_{\xi_c^\pm}^1 d\xi \eta_\pm^2(\xi) \tilde{N}(\epsilon, \xi, z, z_0, t_{dc}) p_\pm'^2(z, \xi). \quad (19)$$

In arriving at this expression we have replaced p_\pm in the product $p_\pm(1-p_\pm)$ by $(1/2) \int_{\xi_c^\pm}^1 d\xi$ while keeping the ξ dependence in the rest of the integrand. This is an approximation neglecting the fluctuations over angles inside the critical cone, and allowing only the total number of phonons within it to fluctuate. Similar expressions can be used to describe the second and the third contributions in (18). If we take a fixed (mean) number of phonons emitted into the critical cone, then

$$\overline{(\delta dM_\epsilon^\pm)^2}|_i = \frac{1}{2} \beta \epsilon^4 d\epsilon \int_{\xi_c^\pm}^1 d\xi \eta_\pm^2(\xi) \tilde{N}(\epsilon, \xi, z, z_0, t_{dc}) p_\pm'(z, \xi) \times [1 - p_\pm'(z, \xi)] \quad (20)$$

and

$$\overline{(\delta dM_\epsilon^\pm)^2}|_t = \frac{1}{2} \beta \epsilon^4 d\epsilon \int_{\xi_c^\pm}^1 d\xi \eta_\pm(\xi) [1 - \eta_\pm(\xi)] \times \tilde{N}(\epsilon, \xi, z, z_0, t_{dc}) p_\pm'(z, \xi). \quad (21)$$

Combining all contributions yields

$$\overline{(\delta dE_{loss}^\pm)^2} = \frac{1}{2} \beta \epsilon^4 d\epsilon \int_{\xi_c^\pm}^1 d\xi \eta_\pm(\xi) p_\pm'(z, \xi) \times [1 - \eta_\pm(\xi) p_\pm p_\pm'(z, \xi)] \tilde{N}(\epsilon, \xi, z, z_0, t_{dc}). \quad (22)$$

The angular distributions of different energy groups are independent, as are also fluctuations for phonons originating from different coordinates z . Hence the cross variances are zero. Thus to obtain the variance of the total energy loss we integrate over ϵ , z , and z_0 , the latter integration accounting for the distribution of phonon absorption sites as in (16), and obtain

$$\overline{(\delta E_{loss}^{\pm})^2} = \frac{1}{2} \int_{-d/2}^{d/2} dz_0 P_s(z_0, E) \int_{-d/2}^{d/2} dz \int_0^{\Omega_D} d\epsilon \beta \epsilon^4 \times \int_{\xi_c^\pm}^1 d\xi \eta_\pm(\xi) p_\pm'(z, \xi) [1 - \eta_\pm(\xi) p_\pm p_\pm'(z, \xi)] \times \tilde{N}(\epsilon, \xi, z, z_0, t_{dc}). \quad (23)$$

We will represent the variance of the energy loss in the form

$$\overline{(\delta E_{loss}^s)^2} = (J_+^s + J_-^s) \epsilon E \quad (24)$$

where $\epsilon \approx 1.7\Delta$ is the mean energy necessary to generate a single QP; this is greater than Δ because of the loss of sub-gap phonons from the system, as discussed earlier. After integrating over z and z_0 we obtain

$$J_\pm^s = \frac{4\Omega_D}{\epsilon} \sum_{m=0}^{\infty} \frac{\kappa(m^2 \xi^2)}{(1 + \delta_{m,0})} \times \frac{(-1)^{m[s+(1\pm 1)/2]} [1 - \exp[im\pi - d/L(E)]]}{\{1 - \exp[-d/L(E)]\} [1 + m^2 \pi^2 L^2(E)/d^2]} \times \int_0^{\Omega_D} \frac{d\epsilon}{\Omega_D} \left(\frac{\epsilon}{\Omega_D}\right)^4 \frac{l_{pb}(\epsilon)}{d} \int_{\xi_c^\pm}^1 d\xi \xi \eta_\pm(\xi) \times \left(\frac{1 - \exp[im\pi - d/l_{pb}(\epsilon)\xi]}{1 + m^2 \pi^2 l_{pb}^2(\epsilon) \xi^2/d^2} - \eta_\pm(\xi) p_\pm(\xi) \frac{2\{1 - \exp[im\pi - 2d/l_{pb}(\epsilon)\xi]\}}{4 + m^2 \pi^2 l_{pb}^2(\epsilon) \xi^2/d^2} \right). \quad (25)$$

Combining Eqs. (16) and (25) we obtain

$$E_{loss}^s = (a_+ J_+^s + a_- J_-^s) \frac{\varepsilon}{\Omega_D} E \quad (26)$$

where the a_{\pm} are constants of the order of unity. Thus we arrive at the important conclusion that the magnitude of the phonon fluctuations that cause uncertainty in the number of generated QPs is directly related to the mean energy loss. Hence by measuring the line shift resulting from QP deficit we may evaluate the parameter $J^s = J_+^s + J_-^s$ defining the phonon noise.

The previous discussion related to QP generation by the first group of phonons, contained within the phonon bubble. However, as described in Sec. I, further phonon generations of successively lower energies are also released, which make contributions to phonon noise that are increasingly less dependent on the coordinates of the photon absorption site, and are not correlated with that for the primary phonons. Contributions from successive phonon generations to the total noise are additive and in principle dependent on photon energy, so that

$$J^s(E) = J_1^s(E) + J_2^s(E) + \dots \quad (27)$$

An estimate of $J_2^s(E)$ can be obtained from the formula (25) by substituting the appropriate expressions for D and t_{dc} and assuming that each Ω_D phonon breaks a Cooper pair and releases two QPs with mean energy of $\Omega_D/2$. For absorber films a few hundreds of nanometers thick, phonons of the second generation already fill the whole of the film, so we may assume that the densities of phonons of third and subsequent generations are homogeneous. Thus to a good approximation we may assume that all their contributions in the formula (27), namely, J_i^s , are independent of photon energy E . Therefore we may simply include these contributions with other statistical noise factors, which are also independent of photon energy, while retaining only $J_1^s(E)$ and $J_2^s(E)$ as energy-dependent terms.

Finally we will consider vertical inhomogeneity in QP generation, by which we mean the dependence of the average number of the generated QPs on the distance of the absorption site from the escape interface. This dependence results in line broadening if there is any spread of absorption sites along the vertical direction. Although vertical inhomogeneity is due to exactly the same process of loss of productive phonons from the absorber that we discussed above, its effect is different from that of phonon noise, giving rise to an inhomogeneous distribution rather than to statistical fluctuations. However we shall now show that under normal experimental circumstances the two contributions can be treated additively.

Let $S(Q)$ be the normalized line shape, that is, the density distribution function for each value of charge output Q . For a fixed absorption depth z_0 the line shape is Gaussian so that

$$S(z_0, Q) = \frac{1}{\sqrt{2\pi}\sigma(z_0)} \exp\left(-\frac{[Q - Q(z_0)]^2}{2\sigma^2(z_0)}\right) \quad (28)$$

where $\sigma^2(z_0)$ is the variance of the signal due to all statistically independent noise sources. For a distribution of absorp-

tion sites with the probability density given by formula (15) we define

$$S(Q) = \int_{-d/2}^{d/2} dz P_s(z, E) S(z, Q) \quad (29)$$

and $\langle Q \rangle$, the mean value of charge output, is given by $\int_0^\infty dQ Q S(Q)$. Hence

$$\begin{aligned} \langle Q \rangle &= \int_{-d/2}^{d/2} dz P_s(z, E) Q(z) \left(1 - \frac{1}{2} \operatorname{erfc} \frac{\sqrt{2}Q(z)}{2\sigma(z)}\right) \\ &+ \int_{-d/2}^{d/2} dz \frac{P_s(z, E)}{\sqrt{2\pi}} \sigma(z) \exp\left(-\frac{Q^2(z)}{2\sigma^2(z)}\right) \end{aligned} \quad (30)$$

which for a typical sharp line with $Q(z) \gg \sigma(z)$ becomes with exponentially high accuracy

$$\begin{aligned} \langle Q \rangle &= \int_{-d/2}^{d/2} dz P_s(z, E) Q(z) \left[1 + \frac{1}{\sqrt{2\pi}} \frac{\sigma^2(z)}{Q^2(z)} \exp\left(-\frac{Q^2(z)}{2\sigma^2(z)}\right)\right] \\ &\cong \int_{-d/2}^{d/2} dz P_s(z, E) Q(z) \equiv \langle Q \rangle_0. \end{aligned} \quad (31)$$

A similar calculation yields for $\langle Q^2 \rangle$ the following result, valid to an exponentially high accuracy:

$$\langle Q^2 \rangle = \int_{-d/2}^{d/2} dz P_s(z, E) [Q^2(z) + \sigma^2(z)] \equiv \langle Q^2 \rangle_0 + \langle \sigma^2 \rangle_0. \quad (32)$$

Correspondingly

$$\begin{aligned} \langle (\delta Q)^2 \rangle &= \langle Q^2 \rangle - \langle Q \rangle^2 \\ &= \int_{-d/2}^{d/2} dz P_s(z, E) Q^2(z) - \left(\int_{-d/2}^{d/2} dz P_s(z, E) Q(z)\right)^2 \\ &+ \int_{-d/2}^{d/2} dz P_s(z, E) \sigma^2(z) = K_v \langle Q \rangle_0^2 + \langle \sigma^2 \rangle_0, \end{aligned} \quad (33)$$

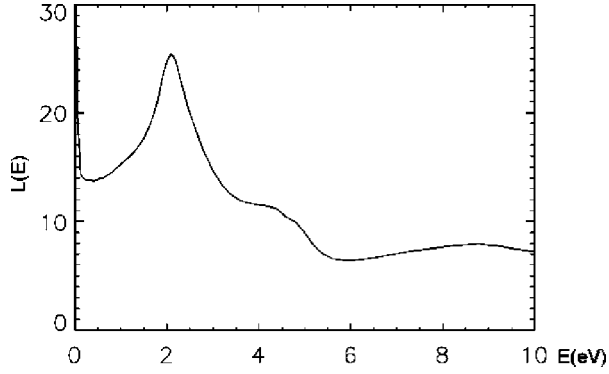
where we have introduced a parameter K_v defined as

$$\begin{aligned} K_v &= \frac{\int_{-d/2}^{d/2} dz P_s(z, E) Q^2(z) - \left(\int_{-d/2}^{d/2} dz P_s(z, E) Q(z)\right)^2}{\left(\int_{-d/2}^{d/2} dz P_s(z, E) Q(z)\right)^2} \\ &\equiv \frac{\langle Q^2 \rangle_0 - \langle Q \rangle_0^2}{\langle Q \rangle_0^2}. \end{aligned} \quad (34)$$

Thus it follows that for any given line shape which results from the superposition of sharp Gaussian functions, the dispersion of energy loss is given by the sum in formula (33). Usually the resulting charge output can be fitted with a Gaussian curve to a sufficiently high accuracy and according to the formula (33) its width Σ is given by

$$\Sigma^2 = K_v \langle Q \rangle_0^2 + \langle \sigma^2 \rangle_0. \quad (35)$$

Finally, writing $Q(z) \sim E - E_{loss}(z)$ and substituting that into the expression (34) we obtain

FIG. 2. Photon absorption length $L(E)$ in Ta.

$$K_v = \frac{\langle E_{loss}^2(z) \rangle_0 - \langle E_{loss}(z) \rangle_0^2}{[E - \langle E_{loss}(z) \rangle_0]^2} \simeq \frac{\langle E_{loss}^2(z) \rangle_0 - \langle E_{loss}(z) \rangle_0^2}{E^2} \quad (36)$$

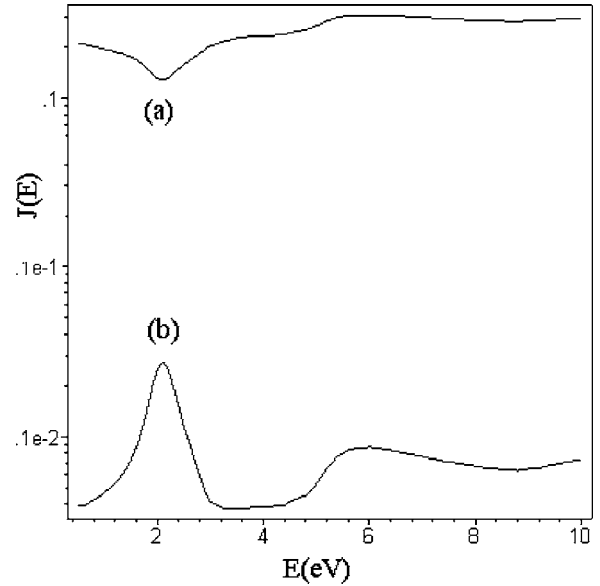
where $E_{loss}(z)$ is given by formula (16) for the relevant direction of photon incidence. The vertical inhomogeneity factor K_v , relating to the total energy loss, is composed of two separate contributions through the near and far interfaces relative to the incident photon. However, for simplicity these will not be shown separately. The importance of the quantity K_v for the modeling of experimental results will be discussed in Sec. V.

IV. ILLUSTRATION OF TYPICAL EFFECTS

In this section we will describe the experimental consequences of phonon escape through the interfaces during energy down-conversion. For comparison with experimental data described in the following section we will focus on the limiting regimes corresponding to the absorption of optical photons and x-ray photons, respectively. For the former, the photon absorption length is much shorter than the layer thickness while for the latter the opposite situation occurs. We will consider initially the Ta/Al₂O₃ interface, for which experimental data have been obtained in both regimes.

A. Shallow absorption: $L(E) \ll d$

First we consider photons in the range 1–10 eV incident along the normal to the interface. Figure 2 shows the photon absorption length $L(E)$ in this energy range in Ta. The strong absorption and dependence on energy give rise to a spatial

FIG. 3. Phonon noise factors J_{\pm}^1 for Ta/Al₂O₃ system as a function of photon energy for (a) the near interface and (b) the distant interface.

variation of density of absorption sites. Table I contains the material parameters that are needed to calculate the phonon noise and vertical inhomogeneity factors J and K_v , as shown in Figs. 3 and 4, respectively, as a function of photon energy. It should be noted that the QP diffusion parameter D , is smaller than the value obtained from electrical conductivity measurements. This is because QP energies in the down-conversion process are higher than the Debye energy, and the mechanism of diffusion is the emission of Brillouin zone boundary phonons, which is a much faster process than conventional elastic scattering. The two curves corresponding to phonon escape through the two interfaces, assumed to be identical (Ta/Al₂O₃), are shown for a photon incident through the (+) interface ($s=1$). As is seen from Fig. 3, for shallow absorption the phonon escape parameters are quite different, and the contribution due to the distant escape interface can be neglected. It is interesting to note that J_{+}^1 has a minimum, while J_{-}^1 has a maximum at $E=2.1$ eV, the energy for which the absorption coefficient has a local minimum. This follows from (26) since J_{\pm}^s is proportional to the energy loss through the corresponding interface. At the absorption minimum an absorption site is further away from the interface of incidence, so that J_{+}^1 is also at a minimum. At the

TABLE I. Material characteristics for Ta/Al₂O₃ interface.

Symbol	Name	Value	Comment
Ω_D	Debye energy in Ta	20.7 meV	
Δ	Energy gap	0.7 meV	
τ_{ph}	Characteristic pair-breaking time	22 ps	From Ref. 14
τ_s	Electron-phonon scattering time above Ω_D	35 fs	From Ref. 2
t_{dc}	Duration of $E_1 \rightarrow \Omega_D$ stage	0.25 ps	Estimated from (9)
D	Diffusion coefficient for electrons with $\epsilon \geq \Omega_D$	1.0 cm ² s ⁻¹	Fitting parameter

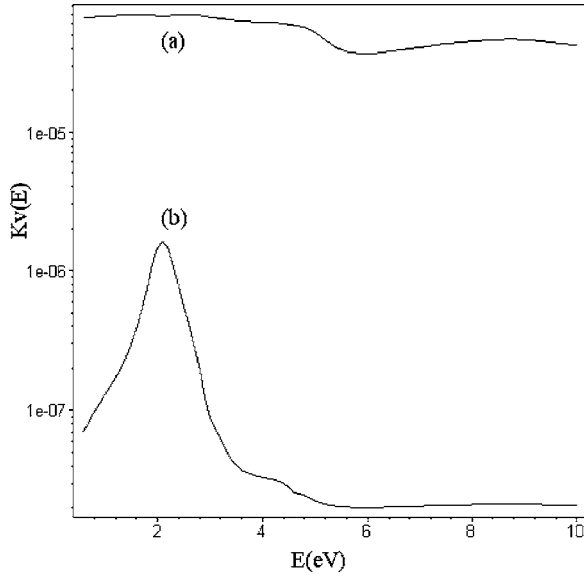


FIG. 4. Vertical inhomogeneity factor K_v for the Ta/Al₂O₃ system as a function of photon energy E for (a) the near (+) interface and (b) the distant (-) interface.

same time this absorption site is closer to the more distant interface, so that J_-^1 is at a maximum.

It is important to note that while the contributions to J for different interfaces are additive, those for K_v are not because of E^2 factor. For shallow absorption the distance from the absorption site to the near escape interface remains smaller than, or of similar magnitude to, the relevant phonon mean free paths; hence there is only a slight variation in the corresponding K_v . The distance to the far interface is much larger, leading to enhanced variation of K_v with E . But for the same reason its absolute value is much smaller.

B. Bulk absorption: $L(E) \gg d$

For most thin film detectors with absorber thicknesses less than $1 \mu\text{m}$ in the x-ray spectral region ($\geq 1 \text{ keV}$) the absorption length is much larger than the film thickness. For this situation the absorption sites are distributed uniformly through the absorber and the initial stage of down-conversion is different from that described earlier. After the initial x-ray absorption there is an additional down-conversion stage from a few keV down to an electron energy in the conduction band around E_1 . The incident photon energy is first transferred to a photoelectron which moves along a slightly curved trajectory, releasing its energy by emitting plasmons and causing secondary ionization. Empirically the photoelectron range R_e in micrometers has the approximate form⁴

$$R_e = \frac{3.52}{\rho_a} \left(\frac{E}{10} \right)^{1.754} \quad (37)$$

where ρ_a is the absorber density in g cm^{-3} and E the photon energy in keV. For a Ta absorber at 6 keV this expression gives $R_e \approx 0.086 \mu\text{m}$. At normal incidence the trajectory of the resulting photoelectron remains approximately parallel to

the interface. However, it experiences elastic Rutherford scattering causing kinks along its track and resulting in initial energy deposition in a volume with a characteristic size which is less than R_e . Thus even in the absence of scattering the excited electrons will develop a small but finite spatial distribution with energies around E_1 along the z axis. To evaluate this distribution we need to calculate the mean free path of electrons with energy of $2E_1$, which is the mean energy of the electron generation immediately above the threshold E_1 . The lifetime of these electrons is $\tau_s/4$, since $\tau_{ee}(E_1) = \tau_s$ and $\tau_{ee} \sim \epsilon^{-2}$. Hence the characteristic spread is of the order of $\bar{v}\tau_s/4$, where \bar{v} is the characteristic electron velocity at E_1 . For Ta, taking $\bar{v} \approx 10^8 \text{ cm/s}$, we obtain a spread of $\geq 5 \text{ nm}$. Thus, in contrast with the pointlike initial electron energy distribution following the absorption of a photon in the range of 1 eV, for x rays there will be a finite spatial distribution of E_1 electrons even before the onset of the $E_1 \rightarrow \Omega_D$ down-conversion cascade.

In contrast also to the earlier situation in which it was assumed that the interface was nontransparent for electrons with energy below E_1 , higher-energy electrons can move freely through an interface. Thus by changing the boundary conditions for (4) from nontransparent to transparent interfaces we can model the z profile of the E_1 electron density after x-ray absorption as

$$\rho_X(z, z_0) = \tilde{A}(z_0) \sum_{m=0}^{\infty} \exp\left(-\frac{m^2 \pi^2 a_0^2}{d^2}\right) \times \sin m\pi \left(\frac{1}{2} + \frac{z}{d}\right) \sin m\pi \left(\frac{1}{2} + \frac{z_0}{d}\right) \quad (38)$$

where a_0 is a parameter describing the spread of the E_1 electron distribution around the absorption depth z_0 along the z axis, and $\tilde{A}(z_0)$ is the normalization constant given by

$$\tilde{A}^{-1}(z_0) = \frac{2d}{\pi} \sum_{k=0}^{\infty} \frac{1}{2k+1} \exp\left(-\frac{(2k+1)\pi^2 a_0^2}{d^2}\right) \times \sin(2k+1)\pi \left(\frac{1}{2} + \frac{z_0}{d}\right). \quad (39)$$

The phonon distribution function in the phonon bubble can be obtained as

$$\tilde{N}_X(z, z_0) = \int_{-d/2}^{d/2} dz' \rho_X(z', z_0) \tilde{N}(z, z'). \quad (40)$$

Correspondingly the energy loss is written as

$$E_{loss}(z_0) = E \tilde{A}(z_0) \sum_{m=0}^{\infty} f_m \sin m\pi \left(\frac{1}{2} + \frac{z_0}{d}\right) \quad (41)$$

where

$$\begin{aligned}
f_m &= \frac{2d}{\pi} \frac{\kappa(m^2\xi^2)}{(1 + \delta_{m,0})} \int_0^1 d\xi \xi \eta(m, \xi) \int_0^{\Omega_D} d\left(\frac{\epsilon}{\Omega_D}\right) \\
&\times \left(\frac{\epsilon}{\Omega_D}\right)^3 \frac{l_{pb}(\epsilon)}{d} \frac{1 - \exp[im\pi - dl_{pb}(\epsilon)\xi]}{1 + m^2\pi^2 l_{pb}^2(\epsilon)\xi^2/d^2} \\
&\times \sum_{m'=0}^{\infty} \frac{m[1 - \cos \pi(m - m')]}{m^2 - m'^2}. \quad (42)
\end{aligned}$$

Using (41), (42), and (34) we may obtain the vertical inhomogeneity factor for x-ray absorption. Results of such a calculation will be given in the next section for a specific ex-

perimental situation. The expressions for the J factors can be obtained for x rays similarly. However in this energy range their effects on detector resolution are negligible compared with inhomogeneous broadening.

V. RESOLUTION IN SUPERCONDUCTING TUNNEL JUNCTION PHOTON DETECTORS

In this section we will discuss the effects of phonon noise and vertical inhomogeneity specifically on the performance of STJ single-photon detectors and make comparison with experimental measurements. The expression for the measured STJ resolution in its most general form is given by

$$\Delta E = 2.355 \sqrt{\left(F + G + H + J(E) \frac{E}{E'}\right) \varepsilon E' + \sigma_{el}^2 + [K_h + K_v(E)] E'^2}. \quad (43)$$

Here F , G and H are Fano, tunnel,^{15,16} and cancellation¹⁷ noise factors, respectively, $J(E)$ corresponds to the effect of phonon noise, σ_{el}^2 is the noise contribution from the experimental electronics, K_h takes account of horizontal variation in response, and $K_v(E)$ is the vertical inhomogeneity factor introduced in Sec. III. Equation (43) takes account of the difference between the deposited energy $E' = E - E_{loss}$ and the photon energy E . Apart from σ_{el}^2 , which is measured directly in a separate experiment using electronic pulses, previous forms of (43) have contained only F , G , H , and K_h . Our proposed modification is thus the incorporation of phonon noise and broadening due to vertical inhomogeneity.

We have obtained strong evidence for the presence of phonon noise from measurements of the resolving power R , defined as $E/\Delta E$, of a STJ photon detector in the optical range. The $30 \times 30 \mu\text{m}^2$ square STJ had a lay-up of 100 nm base Ta, 30 nm Al, AlO_x barrier, 30 nm Al, and 100 nm top Ta, deposited on an r -plane sapphire wafer. The experiments were carried out at a temperature of 285 mK, where the device had a responsivity of $2 \times 10^5 e^-/\text{eV}$ and a pulse decay time of 85 μs . Figure 5 shows the dependence on energy of the measured resolving power. It is seen that a definite change in the slope of the curve occurs at an energy close to the peak of the photon absorption plot, Fig. 2. The dashed curve in Fig. 5 represents the modeled intrinsic resolving power, including contributions from both the phonon noise term $J(E)$ and the vertical inhomogeneity factor $K_v(E)$ modeled for this STJ structure. A convincing correlation is obtained between the energy dependence of $J(E)$ and that of R . Beyond the absorption feature at 2.1 eV, the increasing $J(E)$ matches the relative decrease in R . We believe that this correlation is strong evidence that the phonon noise plays an important role in determining the resolving power of STJ photon detectors in the optical range. The contribution of $K_v(E)$ is not important at the lower portion of the energy range but because of the additional factor of E^2 begins to make a significant ($\approx 18\%$) contribution by 6 eV.

We also carried out experiments in the optical region using a $30 \times 30 \mu\text{m}^2$ square Al-based STJ with the lay-up 100 nm base Al, AlO_x barrier, 50 nm top Al, deposited on r -plane sapphire. In principle an Al STJ should have a significantly higher resolving power than a Ta device because of the lower gap energy, but measured values to date have been hardly different from those obtained for Ta. In our results shown in Fig. 6 the observed linewidth was roughly a factor of 2 larger than the Fano + tunnel limit, obtained from (43) considering only terms with F and G under the square root. This result provides a strong indication that the excess broadening results from phonon noise, the magnitude of which is inversely proportional to the superconducting energy gap, as shown in (25). Although there is no well-defined change of slope of R as seen for Ta, this is not unexpected since the variation of photon absorption coefficient of Al in the optical range is much weaker than for Ta. However, the modeled curve obtained using realistic parameters for Al listed in

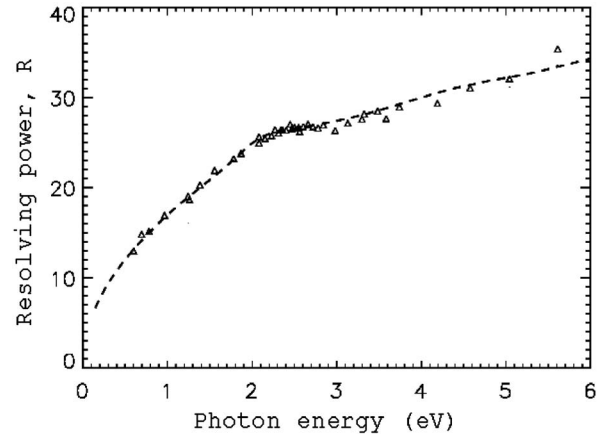


FIG. 5. Fitted model for the resolving power $R = E/\Delta E$ (dashed curve) in a Ta/Al STJ superimposed on the intrinsic measurements (triangles).

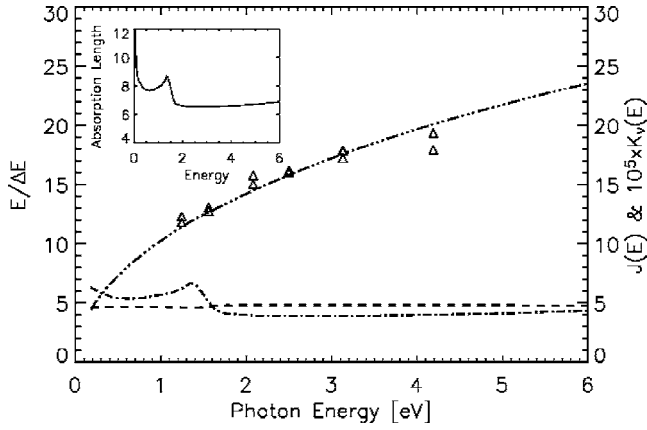


FIG. 6. Fitted model for the energy-resolving power (dash-triple-dotted curve) in Al STJ superimposed on the intrinsic measurements (triangles). Inset: absorption coefficient as a function of photon energy in Al. $K_v(E)$, dash-dotted curve; $J(E)$, dashed curve.

Table II matched closely the measured values in both magnitude and energy dependence.

As noted above, while at energies in the optical range the term $J(E)$ arising from phonon noise dominates the STJ linewidth, at x-ray energies the main source of line broadening, because of the E^2 factor, should be vertical inhomogeneity. The effect of lateral inhomogeneity, characterized by K_h , can be reduced by using a narrow collimated photon beam so that the observed signal originates from a small area. For a Ta STJ at 6 keV the Fano+tunnel noise limited linewidth is calculated to be ≈ 7 eV, but experimentally the best value obtained with a collimated beam is 19 eV.^{21,22} We believe that the additional broadening in Ta STJs can be explained by a varying density of photon absorption sites in a direction normal to the interfaces. We recall from Sec. IV that in addition to vertical inhomogeneity, defined by K_v , the variation depends on the spatial distribution in the z direction of electrons at the end of the down-conversion stage $E_0 \rightarrow E_1$, denoted as a_0 in (38). Unfortunately, this parameter, which depends on the multi-Rutherford scattering of the initial photoelectron, is not accurately known. Nevertheless some information on its magnitude can be obtained by comparison with other work.

In Fig. 7 we plot the calculated resolution (linewidth) at 6 keV due to vertical inhomogeneity as a function of the

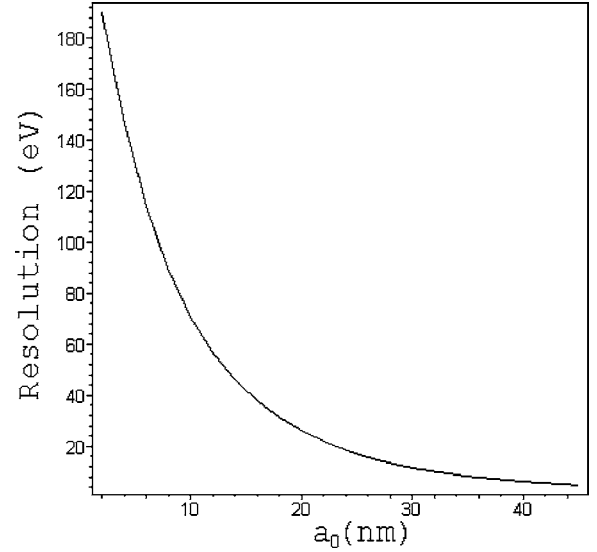


FIG. 7. Calculated line broadening at 6 keV for a Ta STJ on a sapphire substrate.

radius of electronic cloud a_0 , for a Ta/ Al_2O_3 /Ta STJ grown on a sapphire substrate with electrode thickness of 100 nm.²¹ All material parameters are the same as in the Table I. As is seen from this figure, in order to produce 19 eV resolution the value of a_0 would have to be ≈ 25 nm. This value is consistent with observations on Nb STJs based on counting of the number of bridging events in charge output versus signal rise time scatter plots,²³ in which energy deposition either in the base or in the top electrodes results in clearly differentiated areas. For photon absorption events that occur close to the barrier photoelectrons may lose some energy crossing into the neighboring electrode, leading to events intermediate between base and top electrodes. Counting the number of such events yields an estimate for a_0 . To our knowledge the only other experiments that cast any light on this quantity have been the measurements by Frunzio *et al.*²⁴ on a Ta/Si distributed photon detector (DROID) at 5.9 keV. Their measured linewidth was 13.1 ± 1.6 eV, leading, after subtraction (in quadrature) of the electronic contribution (7.6 eV), to an intrinsic linewidth of 10.7 eV. Frunzio *et al.* themselves proposed that, within the experimental uncertainty, this figure was given by a combination of several different effects, Fano noise, trapping multiplication, mul-

TABLE II. Material characteristics for Al/ Al_2O_3 interface.

Symbol	Name	Value	Comment
Ω_D	Debye energy in Al	36.9 meV	
Ω_1	Threshold energy for phonon-controlled cascade in Al	3.3 meV	From Ref. 2
Δ	Energy gap	0.17 meV	
τ_{ph}	Characteristic pair-breaking time	242 ps	From Ref. 14
τ_s	Electron-phonon scattering time above Ω_D	29 fs	From Ref. 2
t_{dc}	Duration of $E_1 \rightarrow \Omega_D$ stage	0.47 ps	Estimated from (9)
D	Diffusion coefficient for electrons with $\epsilon \geq \Omega_D$	$4.2 \text{ cm}^2 \text{ s}^{-1}$	Fitting parameter
G	Tunnel noise parameter	0.45	Calculated (Refs. 19 and 20)
H	Cancellation noise factor	0.12	Calculated (Ref. 18)

TABLE III. Potentially achievable intrinsic resolving power and resolution for Ta- and Al-based STJ detectors.

STJ	Energy	Best achieved	Best predicted
Ta	2 eV	25 ^a (Ref. 1)	28.7 ^c
Ta	6 keV	12 eV ^b (Ref. 24)	3.8 eV ^d
Al	2 eV	15 ^a	43.6 ^c
Al	6 keV	11.7 eV ^b (Ref. 27)	2.5 eV ^d

^aResolving power.

^bResolution.

^cDirect electrode illumination.

^dAbsorber and trap.

multiple tunneling, cancellation, and self-recombination yielding a total of 8.9 eV. Compared to the measured value this leaves a deficit of 5.9 eV unaccounted for. Our own analysis of the experimental arrangement, assuming a value of 25 nm for a_0 , suggests that vertical inhomogeneity might contribute at most as 11 eV. However, this figure is based on our modeling of phonon transmission within the acoustic mismatch model, while the Ta/Si interface contains an embedded, amorphous layer of SiO₂ which will certainly scatter high-frequency phonons back into the absorber,^{10–13,25,26} thus reducing the phonon transmission coefficient and hence the contribution to resolution by a significant factor.

Finally we consider how it might be possible to design an optimized STJ in which phonon noise and vertical inhomogeneity are minimized. Since the magnitudes of these effects are proportional to the fraction of the original photon energy lost as phonons, the main objective must be to reduce this loss as far as possible.

At optical energies the absorption length is smaller than the electrode thickness so that radiation is absorbed strongly in the STJ electrode itself. If the photons are incident from the vacuum side of the STJ most of the resulting phonons will have interacted with QPs long before reaching the interface, thus greatly reducing the phonon noise contribution. However, for reasons of sample preparation and contacting, in all experiments to date the photons have been injected through the sapphire substrate, resulting in the processes as described in our paper. The contribution of phonon noise could be eliminated at a stroke simply by inverting the experimental arrangement. The potential improvements in resolving power resulting from this simple expedient are indicated in Table III. The “best achieved” figures of 25 and 15 for Ta and Al STJs were those obtained in current experiments, and modeled as described in this paper. While the improvement for a Ta STJ is modest, the potential gain for an Al device is almost a factor of 3, the difference being due to less acoustic mismatch between electrode and substrate and the smaller gap of Al.

For x rays the major source of line broadening arises from vertical inhomogeneity due to the variation in distance of the absorption sites from the interface. In order to reduce the effect of this variation we propose the generic design

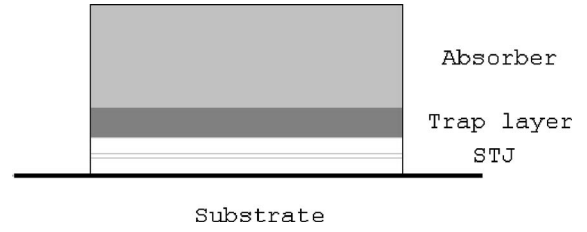


FIG. 8. Schematic design of the composite detector.

shown in Fig. 8. The photon is absorbed in a separate material which is electrically isolated from the STJ, so that energy is injected into the latter in the form of pair-breaking phonons alone and hence no energy is lost to the substrate at the down-conversion stage. Thus, the energetic phonon loss is reduced to zero, since no photon absorption takes place in the STJ itself. The absorber should be a superconductor with a gap $\Delta_a \geq \Delta$ so that recombination phonons in the absorber can break Cooper pairs in the STJ itself. In principle, to optimize detector responsivity, the absorber layer could be as thick as might conveniently be fabricated. However, in this situation the rate at which the down-converted photon energy, divided approximately equally between phonons and QPs in the absorber, was transferred to the STJ would become unacceptably slow. While subgap phonons could escape rapidly, the time scale for the QP energy to be converted into phonons and escape into the STJ would be very long. First, because of the low QP density recombination would be slow. Second, the pair-breaking phonon could be reabsorbed before it reached the interface with the STJ, giving rise to a phonon bottleneck. These problems are avoided by the introduction of a thin QP trapping layer which has an energy gap intermediate between those of the absorber and STJ, of thickness of the order of the coherence length for effective QP recombination. An excess population of QPs will build up in the trap excited by $\geq 2\Delta_a$ phonons from the absorber, whereas the absorber is transparent to recombination phonons generated in the trap. In addition, for $\Delta_a > \Delta$ a large fraction of the population of absorber subgap phonons will also be available for QP excitation in the STJ. This is because of the strong dependence of phonon emission rate on phonon energy, proportional to Ω^3 , leading to a phonon distribution of the subgap phonons in the absorber peaked close to $2\Delta_a$. Thus the effect of the trap is to enhance the fraction of the initial photon energy that is converted into phonons capable of breaking Cooper pairs in the STJ.

It is straightforward to work out the consequent linewidth reduction. Photon absorption and subsequent energy down-conversion inside the absorber result in the fractions of energy $E\Delta_a/\varepsilon_a$ and $E(1-\Delta_a/\varepsilon_a)$ being accumulated in the QP and phonon systems, respectively. Here ε_a is the energy necessary to generate one QP in the absorber. Then the energy deposited into the STJ through phonons becomes $E = sE_0\Delta_a/\varepsilon_a + E_0(1-\Delta_a/\varepsilon_a) = E_0[1 - (1-s)\Delta_a/\varepsilon_a]$, where s is the fraction of the energy of subgap phonons from the absorber which are capable of breaking Cooper pairs in the STJ. If ε is the energy needed to create one QP in the STJ then the total number of generated QPs in the STJ is $E_0/\varepsilon[1 - (1-s)\Delta_a/\varepsilon_a]$ leading to the following formula for

the effective energy required to generate one QP in the STJ following photon absorption in the absorber:

$$\varepsilon_{eff} = \frac{\varepsilon}{1 - (1 - \varsigma)\Delta_a/\varepsilon_a}. \quad (44)$$

Thus $\varepsilon \leq \varepsilon_{eff} \leq \varepsilon/(1 - \Delta_a/\varepsilon_a)$ and assuming that $\varepsilon/\Delta = \varepsilon_a/\Delta_a = 1.75$ we obtain $1.75 \leq \varepsilon_{eff}/\Delta \leq 4.08$. If the device is laterally homogeneous and both phonon noise and vertical inhomogeneity have been eliminated, then the theoretical resolution of the device in Fig. 8 is given by

$$\Delta E = 2.355 \sqrt{(F + G + H)\varepsilon_{eff}E}. \quad (45)$$

The ideal scenario is one in which all the QP energy in the absorber is converted into phonons which break Cooper pairs in the STJ. Then $\varsigma = 1$, ε_{eff} is equal to ε , and the theoretical limit is realized.

In Table III we give the STJ resolution that might be achieved following the considerations discussed in this paper. Our conclusion is that, although phonon noise mechanisms currently make a significant contribution to signal linewidths in both optical and x-ray regions, there is valuable potential for improvement by careful attention to experimental and sample design.

VI. SUMMARY

In this paper we have developed the theory of photoelectron energy down-conversion in superconductors near an interface, and have identified phonon processes that give rise to additional energy loss and fluctuations in the resulting population of excited QPs. The effects occur when a photon is absorbed so close to an interface that some of the phonons generated are lost across the interface before being able to break Cooper pairs. The number of such phonons varies with the depth of the photoabsorption site, giving rise to vertical inhomogeneity. Fluctuations arise in the number of phonons reaching the interface, in the number transmitted and, if the superconductor is acoustically softer than the interface itself, in the number within the critical cone for transmission. An important exemplar of these phenomena, which collectively we have called phonon noise, is the superconducting tunnel junction used as a photon detector. We have shown that all the processes described result in significant broadening of the detected signal. At optical energies the major effect is due to phonon escape noise whilst for x-ray photons vertical inhomogeneity dominates. Quantitative comparison with experimental measurements suggests that phonon noise is the major obstacle to realizing Fano-limited resolution in current STJ photon detectors. On the basis of our model we have been able to make proposals for the future design of optimized device structures.

-
- ¹D. D. E. Martin, P. Verhoeve, A. Peacock, A. G. Kozorezov, J. K. Wigmore, H. Rogalla, and R. Venn, *Appl. Phys. Lett.* **88**, 123510 (2006).
- ²A. G. Kozorezov, A. F. Volkov, J. K. Wigmore, A. Peacock, A. Poelaert, and R. den Hartog, *Phys. Rev. B* **61**, 11807 (2000).
- ³Yu. N. Ovchinnikov and V. Z. Kresin, *Phys. Rev. B* **58**, 12416 (1998).
- ⁴D. Van Vechten and K. S. Wood, *Phys. Rev. B* **43**, 12852 (1991).
- ⁵A. G. Kozorezov, J. K. Wigmore, D. D. E. Martin, P. Verhoeve, and A. Peacock, *Appl. Phys. Lett.* **89**, 223510 (2006).
- ⁶G. M. Eliasberg, *Zh. Eksp. Teor. Fiz.* **61**, 1254 (1971); [*Sov. Phys. JETP* **34**, 668 (1972)].
- ⁷J. J. Chang and D. J. Scalapino, *Phys. Rev. B* **10**, 4047 (1974); **15**, 2651 (1977).
- ⁸J. J. Chang and D. J. Scalapino, *Phys. Rev. Lett.* **37**, 522 (1976).
- ⁹V. F. Elesin and Yu. V. Kopaeu, *Sov. Phys. Usp.* **24**, 116 (1981).
- ¹⁰E. T. Swartz and R. O. Pohl, *Rev. Mod. Phys.* **61**, 605 (1989).
- ¹¹A. G. Kozorezov, J. K. Wigmore, C. Erd, A. Peacock, and A. Poelaert, *Phys. Rev. B* **57**, 7411 (1998).
- ¹²G. Fagas, A. G. Kozorezov, C. J. Lambert, J. K. Wigmore, A. Peacock, A. Poelaert, and R. denHartog, *Phys. Rev. B* **60**, 6459 (1999).
- ¹³P. K. Schelling, S. R. Phillpot, and P. Keblinski, *J. Appl. Phys.* **95**, 6082 (2004).
- ¹⁴S. V. Kaplan, C. C. Chi, D. N. Langenberg, J. J. Chang, S. Yafarey, and D. Scalapino, *Phys. Rev. B* **14**, 4854 (1976).
- ¹⁵C. A. Mears, S. E. Labov, and A. T. Barfknecht, *Appl. Phys. Lett.* **63**, 2961 (1993).
- ¹⁶D. J. Goldie, P. L. Brink, C. Patel, N. E. Booth, and G. L. Salmon, *Appl. Phys. Lett.* **64**, 3169 (1994).
- ¹⁷K. Segall, Ph.D thesis, Yale University, New Haven, CT, 1999.
- ¹⁸G. Brammertz, A. G. Kozorezov, J. K. Wigmore, R. den Hartog, P. Verhoeve, D. Martin, A. Peacock, A. A. Golubov, and H. Rogalla, *J. Appl. Phys.* **94**, 5854 (2003).
- ¹⁹P. Verhoeve, R. den Hartog, A. Kozorezov, D. Martin, A. van Dordrecht, J. K. Wigmore, and A. Peacock, *J. Appl. Phys.* **92**, 6072 (2002).
- ²⁰L. J. Hiller, M. L. van den Berg, and S. E. Labov, *Appl. Phys. Lett.* **79**, 4441 (2001).
- ²¹P. Verhoeve, N. Rando, A. Peacock, A. van Dordrecht, and D. J. Goldie, *Appl. Phys. Lett.* **72**, 3359 (1998).
- ²²P. Verhoeve, N. Rando, A. Peacock, D. Martin, and R. H. den Hartog, *Opt. Eng.* **41**, 1170 (2002).
- ²³D. Lumb (private communication).
- ²⁴L. Li, L. Frunzio, C. M. Wilson, D. E. Prober, A. E. Szymkowiak, and S. H. Moseley, *J. Appl. Phys.* **90**, 3645 (2001).
- ²⁵H. J. Maris, in *Proceedings of Seventh International Conference on Phonon Scattering in Condensed Matter*, edited by M. Meissner and R. O. Pohl (Springer-Verlag, Berlin, 1993), p. 256.
- ²⁶J. K. Wigmore, M. Stokes, and A. G. Kozorezov (unpublished).
- ²⁷G. Angloher, M. Huber, J. Jochum, A. Rüdig, F. v. Feilitzsch, and R. L. Mößbauer, in *Low Temperature Detectors*, edited by F. S. Porter, D. McCammon, M. Galeazzi, and C. K. Stahle, AIP Conf. Proc. No. 605 (AIP, Melville, NY, 2002), p. 23.